The strength of PIN–PMN–PT single crystals under bending with a longitudinal electric field

2011 Smart Mater. Struct. 20 055006

(http://iopscience.iop.org/0964-1726/20/5/055006)

Report Documentation Page

Form Approved
OMB No. 0704-0188

1. REPORT DATE	2. REPORT TYPE	3. DATES COVERED
05 MAY 2011		**00-00-2011 to 00-00-2011**

4. TITLE AND SUBTITLE	5a. CONTRACT NUMBER
The Strength Of PIN-PMN-PT Single Crystals Under Bending With A Longitudinal Electric Field	5b. GRANT NUMBER
	5c. PROGRAM ELEMENT NUMBER
6. AUTHOR(S)	5d. PROJECT NUMBER
	5e. TASK NUMBER
	5f. WORK UNIT NUMBER
7. PERFORMING ORGANIZATION NAME(S) AND ADDRESS(ES) **Naval UnderseaWarfare Center,Newport,RI,02841**	8. PERFORMING ORGANIZATION REPORT NUMBER
9. SPONSORING/MONITORING AGENCY NAME(S) AND ADDRESS(ES)	10. SPONSOR/MONITOR'S ACRONYM(S)
	11. SPONSOR/MONITOR'S REPORT NUMBER(S)

12. DISTRIBUTION/AVAILABILITY STATEMENT
Approved for public release; distribution unlimited

13. SUPPLEMENTARY NOTES
Smart Materials and Structures, Volume 20, Number 5, (May 2011)

14. ABSTRACT

The effect of an electric field on the bending behavior of [001] oriented and poled relaxor Pb(In1/2Nb1/2)O3?Pb(Mg1/3Nb2/3)O3?PbTiO3 (PIN?PMN?PT) single crystals was measured using a four point bending apparatus with a longitudinal electric field applied to the bar during bending. The surface finish and electric field amplitude were observed to affect the bending strength. Polished surfaces improve the tensile strength, while also polishing the edges resulted in a significantly larger increase in strength. Application of a DC electric field in the polarization direction during the tests reduced the strength. The four point bending apparatus also produces both tensile and compressive stress?strain curves for the material. Uniaxial compressive loading with an electric field in the [001] direction was carried out to compare the stress versus strain behavior measured in bending with that measured in uniaxial compression. Although the uniaxial compression behavior displays effects of a rhombohedral to orthorhombic phase transformation, this behavior is not observed on the compressive side in the bend bars.

15. SUBJECT TERMS

16. SECURITY CLASSIFICATION OF:			17. LIMITATION OF ABSTRACT	18. NUMBER OF PAGES	19a. NAME OF RESPONSIBLE PERSON
a. REPORT	b. ABSTRACT	c. THIS PAGE			
unclassified	**unclassified**	**unclassified**	**Same as Report (SAR)**	**9**	

Smart Mater. Struct. **20** (2011) 055006 (7pp) doi:10.1088/0964-1726/20/5/055006

The strength of PIN–PMN–PT single crystals under bending with a longitudinal electric field

P Zhao[1], S Goljahi[1], W Dong[1], T Wu[1], P Finkel[2], R Sahul[3], K Snook[3], J Luo[3], W Hackenberger[3] and C S Lynch[1]

[1] Department of Mechanical and Aerospace Engineering, University of California Los Angeles, 420 Westwood Plaza, Los Angeles, CA 90095, USA
[2] Naval Undersea Warfare Center, Newport, RI 02841, USA
[3] TRS Technologies, 2820 East College Avenue, State College, PA 16801, USA

Received 25 January 2011, in final form 17 March 2011
Published 6 April 2011
Online at stacks.iop.org/SMS/20/055006

Abstract
The effect of an electric field on the bending behavior of [001] oriented and poled relaxor $Pb(In_{1/2}Nb_{1/2})O_3$–$Pb(Mg_{1/3}Nb_{2/3})O_3$–$PbTiO_3$ (PIN–PMN–PT) single crystals was measured using a four point bending apparatus with a longitudinal electric field applied to the bar during bending. The surface finish and electric field amplitude were observed to affect the bending strength. Polished surfaces improve the tensile strength, while also polishing the edges resulted in a significantly larger increase in strength. Application of a DC electric field in the polarization direction during the tests reduced the strength. The four point bending apparatus also produces both tensile and compressive stress–strain curves for the material. Uniaxial compressive loading with an electric field in the [001] direction was carried out to compare the stress versus strain behavior measured in bending with that measured in uniaxial compression. Although the uniaxial compression behavior displays effects of a rhombohedral to orthorhombic phase transformation, this behavior is not observed on the compressive side in the bend bars.

(Some figures in this article are in colour only in the electronic version)

1. Introduction

$Pb(In_{1/2}Nb_{1/2})O_3$–$Pb(Mg_{1/3}Nb_{2/3})O_3$–$PbTiO_3$ (PIN–PMN–PT) is under development to increase the phase stability and temperature range of relaxor rhombohedral single crystals. Results reported in the literature indicate that certain compositions are piezoelectric over a broader range of temperatures than $Pb(Mg_{1/3}Nb_{2/3})O_3$–$PbTiO_3$ (PMN–PT) single crystals [1–6]. This work focuses on the mechanical properties of the PIN–PMN–PT crystals and presents the results of bend testing of PIN–PMN–PT single crystal bars with longitudinal electric field loading during the bending. Although the main purpose of the tests was to identify the effect of an electric field on the tensile strength of the bars, the approach also produced tensile and compressive stress–strain curves. Rather unexpectedly, the nonlinear behavior associated with a compressive stress induced rhombohedral to orthorhombic phase transformation that occurs under uniaxial compression was missing. This observed stress–strain behavior as well as a proposed explanation for the suppression of the phase transformation are presented.

Fracture behavior of ferroelectric materials is well known to be affected by the polarization state of the material. Many authors have reported the effect of polarization on Vicker's indentations, with indentation cracks growing larger perpendicular to the polarization direction. Roedel *et al* [7–10] and other authors [11, 12] have performed experimental fracture mechanics as a function of polarization direction on ferroelectric specimens and found that the polarization direction affects the fracture properties. This includes compact tension specimens to obtain the effect of polarization direction on fracture toughness and the use of bend bars to study *R*-curves and to study v-K behavior [13–16]. Other authors also reported fracture testing as a function of polarization direction [12, 17].

There have been a few fracture experiments done with simultaneous electrical and mechanical loading. Double torsion was used by Koepke *et al* [18] and the electric field was

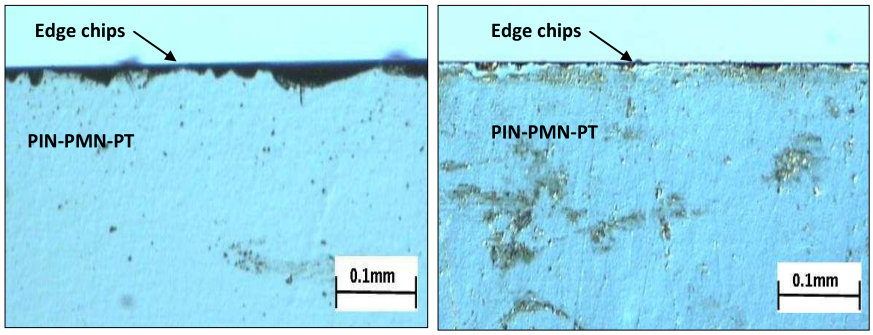

Figure 1. (a) Micrograph of the edge of the first set of bars with only the surfaces polished, and (b) of the second set of bars with the edges also polished.

Table 1. PIN–PMN–PT specimen geometry, surface finish technique and failure stress.

Specimen number	Dimension (mm)	Surface finish	Failure stress (MPa)	Electric field (MV m^{-1})
PIN–PMN–PT 1	3 × 4 × 25	no edges polished	13.5	0.73
PIN–PMN–PT 2	3 × 4 × 25	no edges polished	18.5	0.73
PIN–PMN–PT 3	3 × 4 × 25	no edges polished	21	0
PIN–PMN–PT 4	3 × 4 × 25	no edges polished	22	0
PIN–PMN–PT 5	3 × 4 × 25	no edges polished	26	0
PIN–PMN–PT 6	3 × 4 × 18	edges polished	42	0.5
PIN–PMN–PT 7	3 × 4 × 18	edges polished	47	0.5
PIN–PMN–PT 8	3 × 4 × 18	edges polished	48	0
PIN–PMN–PT 9	3 × 4 × 18	edges polished	70	0
PIN–PMN–PT 10	3 × 4 × 18	edges polished	85	0

shown to change the direction of crack propagation. Several papers [19–22] reported the fracture behavior of ferroelectrics subjected to the mechanical loading and transverse electric field. Su *et al* [23] conducted fracture tests under tensile loading and longitudinal electric field. In all cases, the largest effect of polarization on fracture behavior appears to occur when the crack plane is perpendicular to the polarization.

Compression testing of ferroelectric materials with concurrent electric field loading has been used to characterize the constitutive behavior of a number of ferroelectric materials. Early work of Lynch *et al* [24] presented the uniaxial stress–strain–electric field behavior of lead lanthanum zirconate titanate (8/65/35 PLZT). This technique was later applied to $Pb(Zn_{1/3}Nb_{2/3})O_3$–4.5%$PbTiO_3$ (PZN–4.5%PT) and to PMN–*x*PT [001] cut relaxor single crystals with *x* ranging from 27% to 32%. The single crystal work resulted in clear indications of stress and electric field driven phase transformations [25–29].

2. Experiments

2.1. Specimen preparation

The Bridgman growth technique was used to produce a large PIN–PMN–PT single crystal boule. The orientation of the crystal was determined using an x-ray diffraction system and crystals were cut into bend bars with the [001], [010], and [100] axes oriented with the length, depth and width of the bars. Two different sets of single crystal bars were produced for testing. Dimensions of the first set of bars were 25 mm × 3 mm × 4 mm and dimensions of the second set were 18 mm × 3 mm × 4 mm. Growing the crystals is a time consuming process and obtaining large numbers of bars 25 mm in length turned out to be problematic. The second set of bars was shorter in order to reduce the amount of single crystal material that was used in each test. Bars were cut and polished, and then subjected to bending with and without electric field. The first set of bars had the four larger surfaces polished to a mirror finish, but some small chipping was apparent at the edges as seen in figure 1(a). The second set of bars had the large surfaces polished to a mirror finish, but also had the edges polished. Figure 1(b) shows that the edge chipping was reduced. Wires were attached to the 3 mm × 4 mm surfaces of the polished bars using silver epoxy.

A total of ten specimens were tested, five without edges polished and five with edges polished. Table 1 lists the specimen numbers and the dimensions. Strain gages were mounted to the center of the span on each of the two 4 mm × 25 mm or 4 mm × 18 mm surfaces. These were used to monitor the tensile and compressive strain during the tests. Table 1 also includes the peak loads and electric fields applied to each bar. The applied electric field on the first set of bars was 0.73 MV m^{-1}. On the second of bars, the electric field was reduced to 0.5 MV m^{-1} in order to avoid occasional electrical arcing that destroyed specimens.

A 4 mm × 4 mm × 12 mm single crystal PIN–PMN–PT specimen was produced for compression testing with electric field. Strain gages were mounted at the center of two opposing

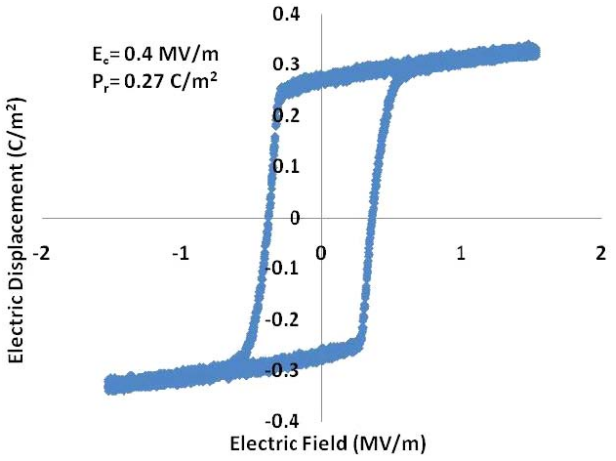

Figure 2. Measured electric displacement D versus electric field E loop of a PIN–PMN–PT crystal.

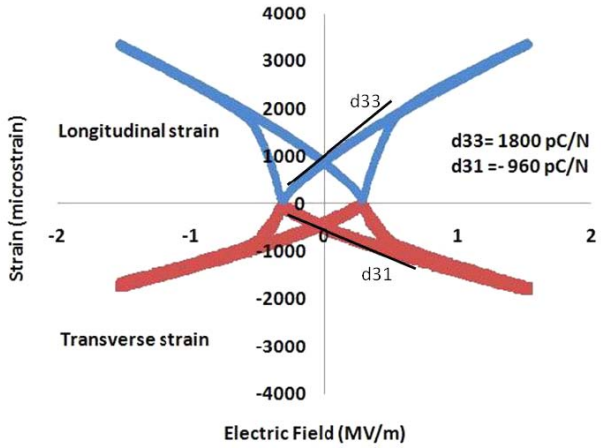

Figure 3. Measured electric field E versus longitudinal and transverse strain ε loop of a PIN–PMN–PT crystal. Note that the remanent strain is zero for this crystal cut and that the curves are offset for clarity.

4 mm × 12 mm surfaces so that longitudinal strain could be measured. The specimen surfaces were not polished. The specimen was baked overnight in a 30 °C oven prior to loading.

2.2. Properties of PIN–PMN–PT

The composition of xPIN–(1-x-y)PMN–yPT is not accurately known for the bars provided and thus is not reported in this work. The composition is rhombohedral and near the rhombohedral to orthorhombic morphotropic phase boundary. Measurements of the physical properties are reported.

2.2.1. Ferroelectric properties. A modified Sawyer–Tower circuit with a [001] oriented PIN–PMN–PT crystal (3 mm × 4 mm × 6 mm) was used to measure the electric displacement versus electric field (D–E) loop (figure 2) and strain versus electric field (ε–E) loop (figure 3). The coercive field E_c was found to be 0.4 MV m^{-1} and the remanent polarization P_r was 0.27 C m^{-2}. Figure 3 shows that the loop of electric field E versus longitudinal and transverse strain ε. The longitudinal strain is along the [001] orientation while the transverse strain is along the [100] orientation on the crystal. By measuring the slope of the loop at electric field $E = 0$, the piezoelectric coefficients were obtained $d_{33} = 1800$ pC N^{-1} and $d_{31} = -960$ pC N^{-1}. Note that the remanent strain is zero for the rhombohedral crystals poled in the [001] direction. The strain versus electric field hysteresis loops are offset in figure 3 for clarity.

2.2.2. Dielectric constant and loss. Dielectric properties of PIN–PMN–PT crystals were measured using HP 4284A LCR meter under multiple frequencies. The dimension of the specimen 3 mm × 4 mm × 1 mm and the poling direction was along the thickness (001) orientation. The relative dielectric constant at the frequency 1 kHz was 1500 and the loss was 0.04.

2.3. Experimental arrangement

2.3.1. Four point bending and associated calculations. The four point bending system is a modification of a device originally developed by Aulbach and Roedel at TU-Darmstadt [7]. The original device utilized a piezoelectric stack actuator to apply load in displacement control. Attention was paid to developing a high stiffness device so that the fracture of brittle materials could be studied under displacement control conditions. The stack actuator in that device did not give sufficient displacement for higher strength and higher compliance specimens, so it was replaced with a highly geared down DC motor in a design that maintained the high stiffness. A schematic of the loading system is shown in figure 4(a). A photograph of the device is shown in figure 4(b). The longer specimens were tested in a device with an inner span of 10 mm and an outer span of 20 mm. The shorter specimens were tested in a device with an inner span of 6 mm and an outer span of 12 mm.

The load cell presses upward on an aluminum oxide block that pushes on the lower rollers. These press on the bottom of the bar being loaded. The upper rollers are constrained by the frame. Wires coming out the sides are used to apply the electric field to the specimen. The apparatus is inverted and placed in an oil bath during testing with the electric field.

Nonlinearities in bending experiments require the use of nonlinear equations found in a textbook by Nadai [30] and first applied to ferroelectric materials by Fett [31–33]. The results of the work reported here displayed linear material behavior and thus the equations of beam theory were applied.

Equation (1) was used to calculate stress σ on the top and bottom of bars.

$$\sigma = \frac{Mc}{I} \tag{1}$$

where M is the bending moment, c is the distance from neutral axis to the outer surface of the bar where maximum stress occurs and I is the area moment of inertia of the cross section.

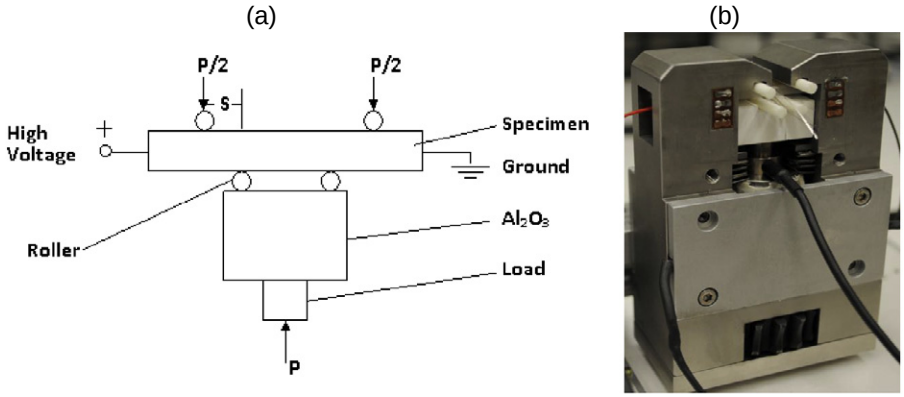

Figure 4. (a) Sketch of the four point bending system with electric field and (b) photograph of the loading apparatus.

The bending moment was calculated using equation (2)

$$M = Ps/2 \tag{2}$$

where P is the load that is applied to the bars and s is the distance between outer and inner rollers (see figure 4(a)).

During the test, the data from the load cell and the Wheatstone bridge strain gage amplifier were recorded. Equation (3) was applied to calculate the load P on the bars.

$$P = \frac{L_o \times g}{0.105} \tag{3}$$

where L_o is the voltage output from the load cell, g is 9.8 m s^{-2} and load cell factor is $1/0.105$ kg V^{-1}.

Equation (4) was applied to covert the signal output from the Vishay strain gage amplifier into microstrain.

$$\varepsilon = \frac{2S_o}{F_g} \times 1000 \tag{4}$$

where S_o is the voltage output from the strain gage amplifier, F_g is strain gage factor, 2.030.

2.3.2. Uniaxial compression with electric field. The compression with electric field measurements were performed using a system located at NUWC Division Newport, similar to the arrangement described in [26]. This system applies concurrent electric field and uniaxial mechanical load to electroactive materials.

Electric field and stress were introduced via the electrodes on the two 4 mm × 4 mm faces of the specimen. Two strain gages were attached in series and the strain measurements were averaged between the two sides to eliminate possible effects from bending moments on the sample. The load frame provided load control in the longitudinal direction so that the specimen was free to move under constant uniaxial stress when the electric field was varied. The stress, strain, electric field, and polarization data were low-pass filtered and recorded through a four channel data acquisition board. A diagram of the experimental arrangement is shown in figure 5.

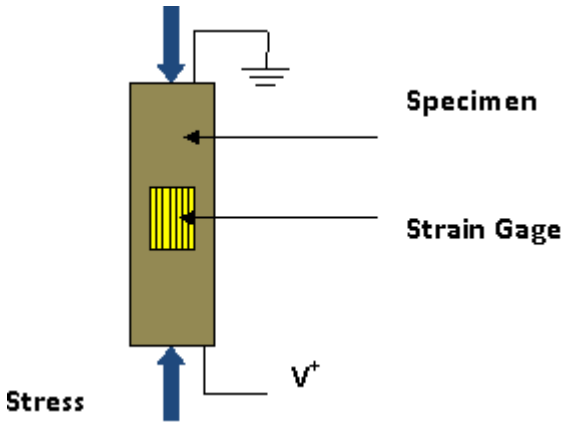

Figure 5. A sketch of the experimental arrangement for concurrent uniaxial compressive stress and electric field loading. Electrical and mechanical loads were applied to the two 4 mm × 4 mm faces. Two strain gages were mounted at the center of two opposing 4 mm × 12 mm faces to measure strain along the length of the specimen.

3. Experimental results

3.1. Bend bar results

In the first set of PIN–PMN–PT crystals, three specimens were tested under bending to failure. The peak stress level at the fracture point ranged from 21 to 26 MPa. Two additional specimens were first subjected to a small mechanical preload followed by an electric field of 0.73 MV m^{-1} and then mechanical loading to failure. The peak stresses were 18.5 and 13.5 MPa.

In the second set of crystals, three specimens were subjected to bending stress until failure. The peak stress level at the fracture point ranged from 48 to 85 MPa. Two specimens were subjected to a small mechanical preload followed by an electric field of 0.5 MV m^{-1} and then mechanical loading to failure. The peak stresses were 42 and 47 MPa.

The measured stress–strain curves presented below do not show error bars. The error in the instrumentation is less than 1% and error bars would be about the same size as the data markers.

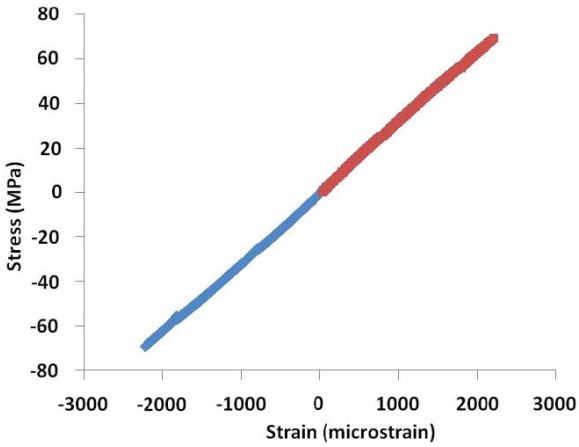

Figure 6. The measured stress versus strain curve with electric field $E = 0$.

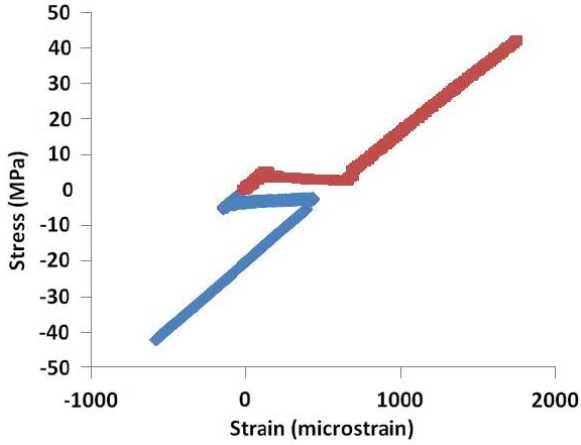

Figure 7. The measured stress versus strain curve with electric field $E = 0.5$ MV m^{-1} applied after a small mechanical preload followed by mechanical loading to failure.

Figure 6 shows the measured tensile and compressive stress and strain curves from a crystal under bending stress with no electric field. The behavior is linear and symmetric in tension and compression. The peak stress and strain at the fracture point were 70 MPa and 2100 $\mu\varepsilon$ for this specimen.

Figure 7 shows the measured tensile and compressive stress and strain behavior for a crystal with a bias electric field applied. A small preload of 3 MPa was applied to the specimen and the tensile and compressive stress and strain relation exhibited linear behavior. Next an electric field of 0.5 MV m^{-1} was applied. The tensile and compressive strain both increased (bar extension) with the electric field increasing. Note that the tensile side of the bar elongated more than the compressive side of the bar. The application of electric field in the presence of a small bending moment increased the curvature of the bar. Finally, mechanical loading was applied until the specimen failed. The crystal displayed linear behavior during the mechanical loading. The peak stress at the fracture point was 42 MPa. The tensile strain and compressive strain at the fracture point were 1800 and -580 $\mu\varepsilon$. The tensile strain was larger than the compressive strain since the electric field caused the extension of the crystal along the longitudinal direction. The decrease of stress as the electric field was applied was due to the reduction in cross sectional dimensions perpendicular to the electric field associated with d_{31}, and the stiff loading apparatus.

3.2. Compression with electric field results

Data was recorded for stress driven strain at several different constant bias electric field levels at room temperature. Table 2 defines the test parameters. The stress cycle consisted of one half of a triangle wave from a load of -0.63–68.75 MPa and back with a loading rate of 10 N s^{-1}.

Figure 8 shows plots of the results of the compression with electric field experiment. At zero electric field, there is a strong nonlinearity at around 40 MPa. This nonlinearity decreases as the electric field is increased. At 0.2 MV m^{-1}, the nonlinearity is almost absent in the mechanical loading range.

Table 2. Test conditions for II-33 mode specimen.

Electric field (kV m^{-1})	Stress (MPa)
0	$-0.63 \rightarrow -68.75 \rightarrow -0.63$
41.67	$-0.63 \rightarrow -68.75 \rightarrow -0.63$
83.33	$-0.63 \rightarrow -68.75 \rightarrow -0.63$
125	$-0.63 \rightarrow -68.75 \rightarrow -0.63$
166.67	$-0.63 \rightarrow -68.75 \rightarrow -0.63$
208.33	$-0.63 \rightarrow -68.75 \rightarrow -0.63$

4. Discussion

Figure 9 shows a bar chart of the specimen failure strength sorted in ascending order. The electric field is shown on the same plot to indicate which specimens had an electric field applied. The first five specimens without polished edges displayed the lowest tensile strength. The average strength of the polished specimens was more than two times that of the unpolished specimens. The electric field consistently reduced the strength of both sets of bars.

The behavior of the material in compression under bending load and under uniaxial load was considerably different. In bending the compressive stress versus strain behavior was linear whereas in uniaxial compression there was a distinct nonlinearity associated with a phase transformation from rhombohedral to orthorhombic symmetry. It appears that the suppression of the phase transformation in bending is the result of constraints placed on the bars by the bending geometry. These constraints occur from both the depth of the specimen and from strain gradients through the thickness of the specimen.

The stress field in the four point bending geometry is depicted in figure 10. This geometry results in tensile stress at the top and compressive stress at the bottom of the bar as shown. When the material at the top of the bar is elongated by the tensile stress, there must be an associated out of plane contraction associated with the Poisson's ratio. Similarly, on the compressive side of the bar there must be an out of plane expansion. This leads to an anticlastic shape of the cross

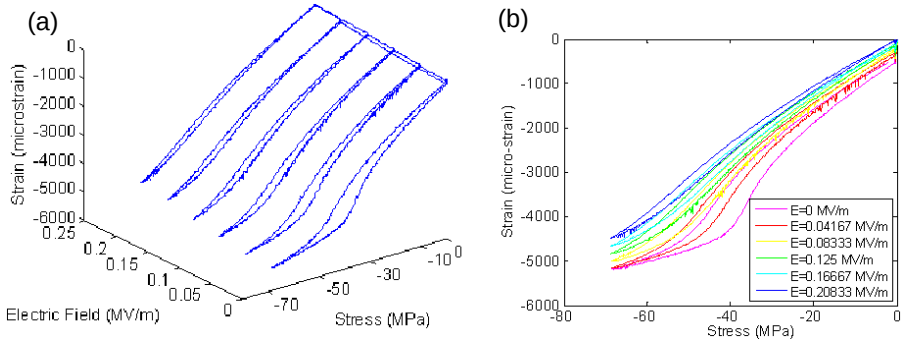

Figure 8. Measured uniaxial compressive stress and strain behavior for a PIN–PMN–PT crystal at different bias electric fields shown in (a) 3D and (b) 2D.

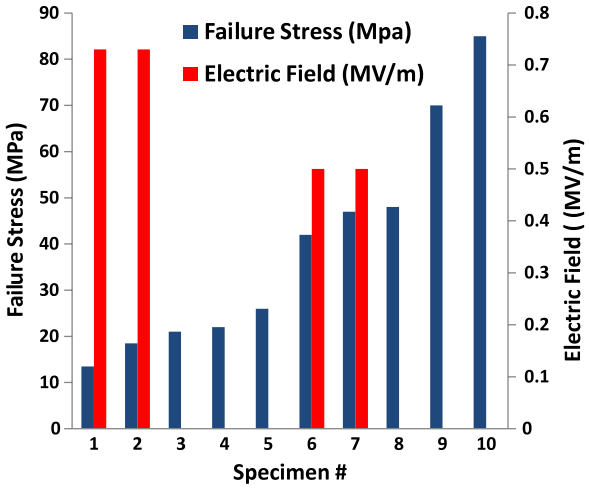

Figure 9. Plot of the strength of the bending bars with unpolished edge (specimens 1–5) and polished edge (specimens 6–10). An electric field of 0.73 MV m^{-1} was applied to specimens 1 and 2. No electric field was applied to specimens 3–5 and 8–10. An electric field of 0.5 MV m^{-1} was applied to specimens 6 and 7.

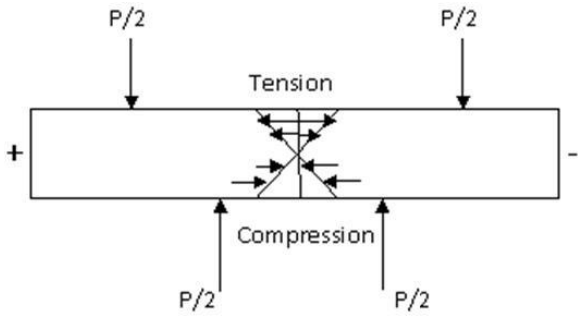

Figure 10. Stress that occurs in a bar subjected to four point bending.

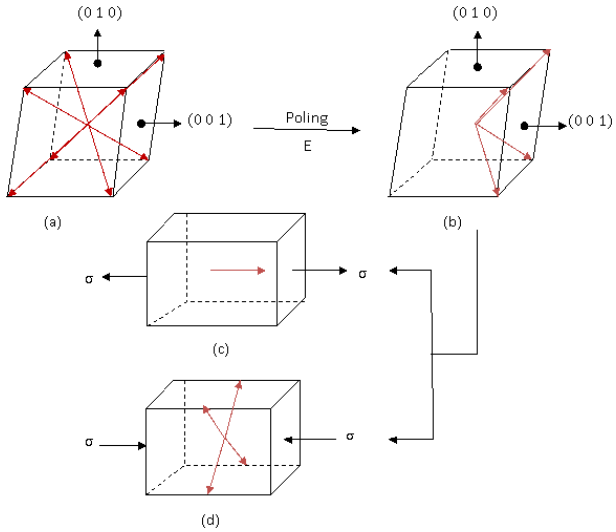

Figure 11. Phase transformation and crystal variants. (a) [001] cut crystal with rhombohedral structure; (b) after poling; (c) tetragonal structure under tension; (d) orthorhombic structure under compression.

section. Thin plates in bending have a 'snap through behavior' at a critical strain level that changes the deformation from the initial anticlastic shape (potato chip) to a uniform strain through the thickness. This is typically zero strain in the out of plane direction in a linear elastic deformation. Many of the bars had both longitudinal and transverse strain gages on the top and bottom surfaces. These strain gages indicated an out of plane Poisson's ratio contraction on the top surface and out of plane expansion on the bottom surface that is consistent with the beam theory analysis. This is also indicative of a state of uniaxial stress at both the top and bottom surfaces, so one would expect a phase transformation at the same stress level in both the bending and the uniaxial compression tests.

Attention is now turned to possible effects of the crystal structure interacting with the geometry that may induce constraints on the phase transformation in bending. PIN–PMN–PT single crystals have a rhombohedral structure. The [001] cut crystal has eight possible rhombohedral variants as depicted in figure 11(a). After poling with an electric field along the length of the bar in the [001] direction, four of the crystal variants are populated (figure 11(b)). Large electric field loading in the [001] direction in PMN–32%PT crystals results in a rhombohedral to tetragonal phase transformation with a large elongational strain (figure 11(c)). Compressive loading in the [001] direction results in a rhombohedral to orthorhombic phase transformation with a large associated contractional strain (figure 11(d)). This is

similar to the behavior of PMN–PT single crystals [26, 28] and the previously measured field driven phase transformation behavior of PIN–PMN–PT single crystals [29] under combined electric field and stress. Based on the compression data at zero electric field, a rhombohedral to orthorhombic phase transformation was expected to occur on the compression side of the bend bar once the stress exceeded 40 MPa. However, this behavior was not observed during any of the bending tests.

The compressive stress induced phase transformation depicted in figure 11(d) involves a contraction in the stress direction and an expansion in the transverse directions. If we now consider a thin sheet of material on the compressive side of the beam, the phase transformation requires that the material expand in the out of plane direction. With the crystal [001], [010], [100] orientations aligned with the length, depth and width of the bar, all of the rhombohedral to orthorhombic transformation systems require an out of plane expansion. This is constrained by the untransformed material slightly deeper into the beam. This geometric constraint explains the observed suppression of the phase transformation when the single crystals are loaded in bending.

Since the crystals are brittle oxide materials, their strength is governed by fracture mechanics. The largest crack-like flaw governs failure in tension. Equation (5) gives the relationship between fracture toughness and failure stress σ^{∞} for a Mode I crack in an elastic material.

$$\sigma_{\text{fail}} = \frac{K_{\text{Ic}}}{f\sqrt{\pi a}} \tag{5}$$

where K_{Ic} is the mode I fracture toughness, f is a factor that depends on crack geometry and is typically around one, and a is the crack length. This equation indicates that as the flaw sizes in the specimen are reduced through polishing, the tensile strength goes up. This is consistent with the observed increase of tensile strength when the edges of the bars were polished, reducing the size of the initial crack-like flaws in the specimens. The electric field across the flaws decreases the fracture toughness. In these experiments the flaws are not controlled, making it difficult to discuss the electric field contributions to fracture quantitatively.

5. Conclusions

Two sets of bars were produced for bending with and without electric field. One set had the large surfaces polished and the second set had the edges polished as well. Polishing the edges reduced the size of the surface flaws present and thus increased the failure strength. Application of an electric field interacted with the surface flaws and reduced the failure strength. Although insufficient tests were run to enable a more detailed statistical analysis of the results, the effects were quite large. Polishing can increase the strength of the bars by a factor of two or more and an electric field can reduce the strength by a similar factor.

The constraint of the phase transformation by the bending geometry was not anticipated and has ramifications for possible transformation toughening associated with domain switching or phase transformations in the region near a crack tip. The crack tip region is typically in a state of plane strain with a high degree of geometric constraint on the out of plane deformation except very near the location where the crack intersects the surface. The results of this work suggest that there will be little or no transformation toughening of the cracks that lead to failure. It is possible that rotating the crystal cut of the beam 45° about its long axis so that the [011] orientations are aligned perpendicular to the compressive stress direction would remove the geometric constraint and allow the transformation to take place at both the tensile and the compressive surfaces. If this is the case, there may also be an orientation dependent component of transformation toughening. These are topics for future investigation.

Acknowledgments

The authors would like to thank TRS Technologies for supporting this work through an SBIR from the US Office of Naval Research (ONR), grant N00014-09-C-0488. PF would also like to acknowledge full support by ONR.

References

[1] Zhang S *et al* 2009 *J. Appl. Phys.* **105** 104506
[2] Zhang S *et al* 2008 *J. Appl. Phys.* **104** 064106
[3] Lee H J *et al* 2010 *Adv. Funct. Mater.* **20** 3154
[4] Liu X *et al* 2009 *J. Appl. Phys.* **106** 074112
[5] Liu X *et al* 2010 *Appl. Phys. Lett.* **96** 012907
[6] Wang X *et al* 2010 *Mater. Sci. Eng.* B **170** 1
[7] Dos Santos e Lucato S L *et al* 2002 *J. Mech. Phys. Solids* **50** 2333
[8] Kounga Njiwa A B *et al* 2006 *Eng. Fract. Mech.* **73** 309
[9] Kounga Njiwa A B *et al* 2007 *Acta Mater.* **55** 675
[10] Oates W S *et al* 2004 *J. Am. Ceram. Soc.* **87** 1362
[11] Jones J L, Salz C R J and Hoffman M 2005 *J. Am. Ceram. Soc.* **88** 2788
[12] Kolleck A, Schneider G A and Meschke F A 2000 *Acta Mater.* **48** 4099
[13] Karastamatis T *et al* 2003 *J. Euro. Ceram. Soc.* **23** 1401
[14] Dos Santos e Lucato S L *et al* 2001 *Acta Mater.* **49** 2751
[15] Chen W *et al* 2001 *J. Am. Ceram. Soc.* **84** 593
[16] Dos Santos e Lucato S L 2003 *J. Am. Ceram. Soc.* **86** 1037
[17] Meschke F, Kolleck A and Schneider G A 1997 *J. Eur. Ceram. Soc.* **17** 1143
[18] Koepke B G and McHenry K D 1979 *Ferroelectrics* **28**
[19] Heyer V *et al* 1998 *Acta Mater.* **46** 6615
[20] Gehrig F, Jelitto H and Schneider G A 2008 *Acta Mater.* **56** 1359
[21] Ma W and Cross L E 2003 *Appl. Phys. Lett.* **82** 3293
[22] Zhang Y, Cheng X and Qian R 2003 *Mater. Sci. Eng.* A **351** 81
[23] Su Y J *et al* 2004 *Acta Mater.* **52** 3753
[24] Lynch C S 1996 *Acta Mater.* **44** 4137
[25] Liu T, Lynch C S and McLaughlin E A 2007 *J. Intell. Mater. Syst. Struct.* **18** 409
[26] McLaughlin E A, Liu T and Lynch C S 2005 *Acta Mater.* **53** 4001
[27] McLaughlin E A, Liu T and Lynch C S 2004 *Acta Mater.* **52** 3849
[28] Liu T and Lynch C S 2006 *Continuum Mech. Thermodyn.* **18** 119
[29] Finkel P, Robinson H, Stace J and Amin A 2010 *Appl. Phys. Lett.* **97** 122903
[30] Nadai A (ed) 1950 *Theory of Flow and Fracture of Solids* (New York: McGraw-Hill)
[31] Fett T *et al* 1998 *J. Mater. Sci. Lett.* **17** 261
[32] Fett T, Munz D and Thun G 1998 *J. Am. Ceram. Soc.* **81** 269
[33] Fett T, Munz D and Thun G 1998 *J. Mater. Sci. Lett.* **18** 1899